

RESEARCH

Open Access



# Polymer lipid hybrid nanoparticles encapsulated with Emodin combined with DOX reverse multidrug resistance of breast cancer via IL-6/JAK2/STAT3 signaling pathway

Honghui Gu<sup>1†</sup>, Fansu Meng<sup>2†</sup>, Haidong Sun<sup>3†</sup>, Lina Yang<sup>1</sup>, Qi Li<sup>1</sup>, Zhong Chen<sup>1</sup>, Tiange Cai<sup>4\*</sup>, Zhenjiang Yang<sup>1\*</sup> and Yu Cai<sup>5\*</sup>

<sup>†</sup>Honghui Gu, Fansu Meng and Haidong Sun contribute equally to this work.

\*Correspondence: caitiange@163.com; dzjysz@163.com; caiyu8@sohu.com

<sup>1</sup> Shenzhen Traditional Chinese Medicine Hospital, Shenzhen 518033, Guangdong, China

<sup>2</sup> Zhongshan Hospital of Traditional Chinese Medicine Affiliated to Guangzhou University of TCM, Zhongshan 528400, Guangdong, China

<sup>3</sup> Department of Surgery, Shenzhen Hospital (Futian) of Guangzhou University of Chinese Medicine, Shenzhen 518034, Guangdong, China

<sup>4</sup> College of Life Sciences, Liaoning University, Shenyang 110036, Liaoning, China

<sup>5</sup> Guangdong Key Lab of Traditional Chinese Medicine Information Technology/International Cooperative Laboratory of Traditional Chinese Medicine Modernization and Innovative Drug Development of Ministry of Education (MOE) of China/School of Pharmacy, Jinan University, Guangzhou 510632, Guangdong, China

## Abstract

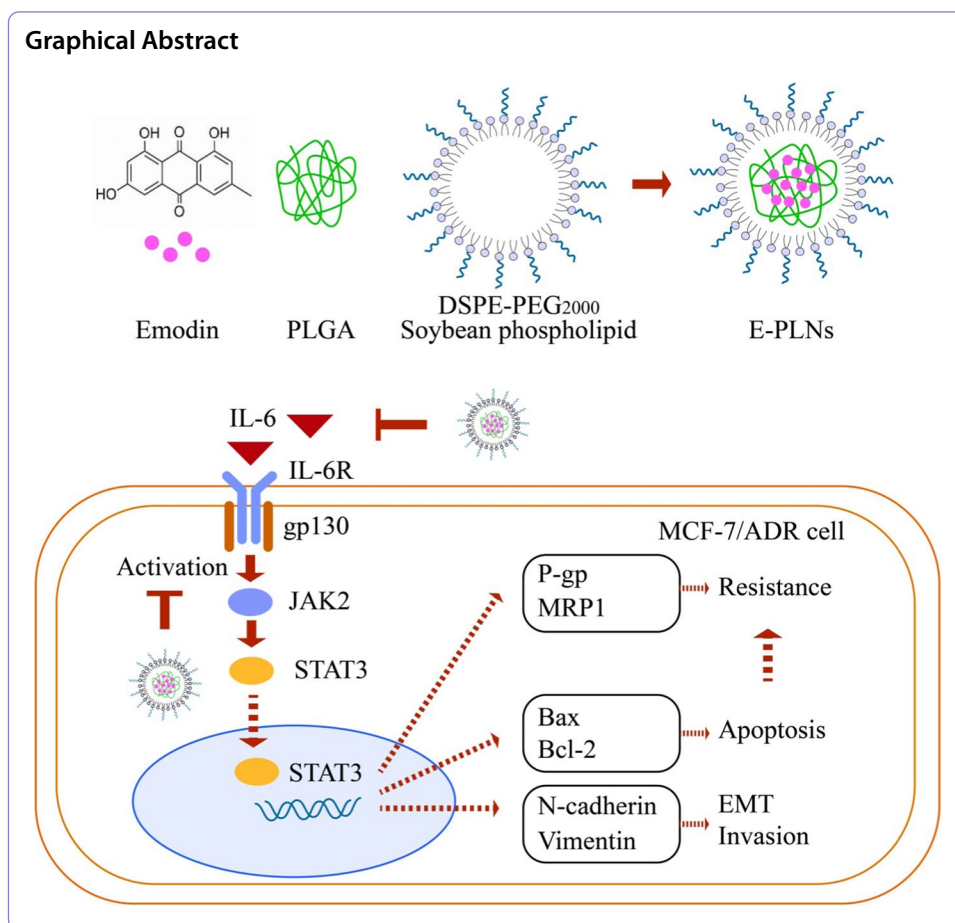
Multidrug resistance (MDR) is one of the main reasons affecting the efficacy of chemotherapy in breast cancer (BC). Our previous studies constructed polymer lipid hybrid nanoparticles encapsulated with Emodin (EMO) (E-PLNs) and proved that they can inhibit epithelial mesenchymal transition (EMT) and reverse MDR in BC. This study aims to explore the mechanisms by which the EMT involved in MDR and the E-PLNs exerted effects. The prepared E-PLNs were characterized by Dynamic light scattering, infrared spectroscopy, X-ray, and differential scanning calorimetry. The effects of drugs or treatments were evaluated by detecting cell viability, apoptosis, invasion, EMT markers, and MDR related proteins in vitro. The results showed that IL-6 could promote proliferation, EMT, invasion and MDR of MCF-7/ADR cells (induced from MCF-7 cells) by activating the JAK2/STAT3 signaling pathway, and these effects could be reversed by AG490 (JAK2 inhibitor) or E-PLNs combined with Doxorubicin (DOX). E-PLNs might be an effective MDR reversal agent for BC.

## Summary

Polymer lipid hybrid nanoparticles encapsulated with Emodin had good physical and chemical properties, improving the bioavailability and efficacy of Emodin. Compared with parental MCF-7 cells, MCF-7/ADR cells overexpressed markers of epithelial mesenchymal transition (EMT), and Galunisertib (EMT inhibitor) inhibited EMT and reversed MDR. Compared with parental MCF-7 cells, MCF-7/ADR cells secreted high level of IL-6. Exogenous IL-6 promoted proliferation, invasion, EMT, and MDR of MCF-7/ADR cells by activating the JAK2/STAT3 pathway. AG490 (JAK2 inhibitor) and/or E-PLNs combined with DOX downregulated the IL-6/JAK2/STAT3 pathway and inhibited its mediated proliferation, invasion, EMT, and MDR in MCF-7/ADR cells.

**Keywords:** Breast cancer, Multidrug resistance, Nanoparticles, Emodin, Epithelial mesenchymal transition





### Introduction

Breast cancer (BC) is one of the tumours with the highest morbidity and mortality rates in women worldwide (Fisusi and Akala 2019). Chemotherapy remains the main treatment for BC (Waks and Winer 2019). However, BC develops multidrug resistance (MDR) during the treatment process, leading to chemotherapy failure (Liu et al. 2021a, Gottesman et al. 2002). Despite various efforts to restore the sensitivity of existing chemotherapeutic drugs and overcome MDR in BC, existing treatments still do not provide sufficient solutions to MDR (Ji et al. 2019).

The mechanisms of MDR in BC are complex and have not been fully elucidated. Currently reported potential mechanisms of MDR include ABC transporter family, cancer stem cell regulation, DNA damage and repair, epigenetic regulation, and epithelial mesenchymal transition (EMT) (Wu et al. 2014). EMT is a transient and reversible cell dedifferentiation process that includes three phases of epithelial, partial EMT and mesenchymal cell states. It was found that a partial EMT state contributed to chemoresistance in BC cells (Lüönd et al. 2021). It was confirmed that BC micro-environment was an (Interleukin 6) IL-6-rich paracrine or autocrine inflammatory environment, and the IL-6/janus kinase 2 (JAK2)/signal transducer and activator of transcription 3 (STAT3) signaling pathway were associated with BC proliferation and migration, and were potential therapeutic targets (Cheng et al. 2020, Shen et al. 2022,

Xu et al. 2020). However, the relationship between autocrine and paracrine IL-6 and downstream JAK2/STAT3 signaling pathway with EMT and MDR in BC remains to be further elucidated.

Emodin (EMO), a natural anthraquinone derivative, has a wide range of pharmacological effects, such as antiviral, antibacterial, antiallergic, antiosteoporosis, immune regulation, and neuroprotection (Dong et al. 2016). In recent years, EMO has been regarded as an inhibitor of protein tyrosine kinase and an anticancer agent with activity against a variety of tumor cells, including lung cancer, BC, liver cancer and ovarian cancer cells (Semwal et al. 2021, Ponnusamy et al. 2020, Li et al. 2020). Despite the potential of EMO as a therapeutic adjuvant to reverse MDR in BC, poor water solubility and unelaborated mechanisms have limited its application.

Nanodrug delivery systems have been widely studied for tumor therapy, which not only enable encapsulation, modification, targeted delivery, and controlled release of therapeutic agents, but can also overcome MDR (Gote et al. 2021, Liu et al. 2022a, Lan et al. 2021, Liu et al. 2021b, Li et al. 2021, Fu et al. 2020). In our previous studies, Emodin-loaded polymer-lipid hybrid nanoparticles (E-PLNs) were prepared optimally, and their inhibitory effect on the growth of BC was confirmed through in vivo and in vitro experiments (Liu et al. 2021c, Zou et al. 2021).

In this study, E-PLNs were prepared and characterized to evaluate its effect on reversing MDR in MCF-7/ADR cells. Besides, the relationship between EMT, IL-6/JAK2/STAT3 signaling pathway and MDR in MCF-7/ADR cells was verified, as well as the regulatory role of E-PLNs combined with chemotherapy drug Doxorubicin (DOX).

## Materials and methods

### Preparation of E-PLNs

E-PLNs were prepared as reported previously (Liu et al. 2021c), which included the following three steps. First, Emodin (3 mg) (Chengdu Prefa Co., Ltd., China) and poly (lactic-co-glycolic acid (PLGA, 20 mg) (Jinan Daigang Bioengineering Co., Ltd., China) were dissolved in 4 mL acetone (Tianjin Comeo Chemical Reagent Co., Ltd., China) to form organic phase. Second, the aqueous phase was prepared by soya phospholipid (40 mg) and distearyl phosphatidyl ethanolamine-polyethylene glycol 2000 (DSPE-PEG2000, 9 mg) (Avituo (Shanghai) Pharmaceutical Technology Co., Ltd., China) reacted in 32 mL 2.5% Pluronic F68 (Beijing Solarbio Science , Technology Co., Ltd., China) solution with stirring at 75 °C water bath at 800 rpm for 3 min. Third, the organic phase was drop-wise injected in aqueous solution at a 75 °C water bath with stirring at 800 rpm for 50 min to remove the organic solvent and the solution was centrifuged at 1000 rpm for 5 min to obtain the E-PLNs which was in the precipitate. The obtained E-PLNs were freeze-dried with 8% mannitol as protectant.

### Determination of EMO encapsulation efficiency and loading efficiency in E-PLNs

The content of EMO in the sample was detected by high performance liquid chromatography (HPLC) (1260, Agilent Technologies Co. Ltd., California, USA) using the external standard method. EMO standards (Beijing Zhongke Quality Inspection Biology Co., Ltd., Beijing, China) were dissolved in methanol (Beijing Merida Technology Co., Ltd., Beijing, China) and prepared at different concentrations. Methanol and E-PLNs

dispersion were mixed in equal volumes (E-PLNs mass was  $M$ ), sonicated for 10 min and filtered with 0.45  $\mu\text{m}$  filtration membrane. The components of the standards and sample solutions were separated on a C18 reverse phase chromatography column (Agilent ZORBAX SB, 4.6 mm  $\times$  250 mm, 5  $\mu\text{m}$ ). The flow rate was 1.0 mL/min, the injection volume was 10  $\mu\text{L}$ , and the column temperature was 30  $^{\circ}\text{C}$ . The mobile phase was methanol:0.1% phosphoric acid solution (V/V, 75:25). The UV detector monitored at 329 nm. The detected mass of EMO in E-PLNs was  $M_t$ . The same volume of the same batch of E-PLNs dispersion (E-PLNs mass is  $M$ ) was placed in an ultrafiltration tube (MWCO = 30 KDa), centrifuged at 12,000 rpm for 30 min, filtered with a 0.45  $\mu\text{m}$  filter membrane, and the filtrate was adjusted to 1 mL. The mass of free EMO was determined as  $M_f$  by HPLC. Equations (1) and (2) were used to calculate the encapsulation efficiency (EE) and load efficiency (LE) of EMO in E-PLNs.

$$\text{EE (\%)} = (M_t - M_f)/M_t \times 100\% \quad (1)$$

$$\text{DL (\%)} = (M_t - M_f)/M \times 100\% \quad (2)$$

#### Particle size and Zeta potential distribution

The polydispersion coefficient (PDI), particle size distribution and Zeta potential distribution of E-PLNs were detected by nanometer particle size meter (Zetasizer Nano ZS90, Malvern Panaco, Malvern, UK).

#### Ultraviolet absorption

Using methanol and phosphate buffer solution (PBS) as blank controls, the absorption spectra of 40  $\mu\text{g/mL}$  EMO methanol solution and PBS containing appropriate concentrations of PLNs, E-PLNs, and PLNS-EMO physical mixture in the range of 200–800 nm were measured by UV–visible spectrophotometer (Cary 60 UV–Vis, Agilent Technologies Co. Ltd., California, USA).

#### Fourier transform infrared spectrometer (FTIR) scan

The appropriate amount of EMO, PLNs, E-PLNs, PLNS-EMO physical mixture was mixed evenly with dried potassium bromide powder in a mortar, and the samples were scanned in the range of 4000–400  $\text{cm}^{-1}$  using a Fourier transform infrared spectrometer (FTIR-8400, Shimadzu, Tokyo, Japan).

#### X-ray polycrystal diffraction (XRD) analysis

An appropriate amount of physical mixture of EMO, PLNs, E-PLNs, and PLNS-EMO were detected by an X-ray polycrystal diffractometer (D8 DISCOVER, Bruker, Massachusetts, USA) with the scanning range from 5 $^{\circ}$  to 90 $^{\circ}$  at the scanning speed of 2 $^{\circ}$ /min.

#### Differential scanning calorimetry (DSC) analysis

Thermal analysis (DSC) of EMO, PLNs, E-PLNs and PLNS-EMO were performed on differential scanning calorimeter (DSC204F1, NETZSCH-Geratebau GmbH, Selb, Germany) in the temperature range of 0–600  $^{\circ}\text{C}$ .

### **In vitro stability study of E-PLNs**

After filtering an appropriate amount of E-PLNs dispersion, add an equal amount of E-PLNs to PBS solution, RPMI1640 medium and RPMI1640 medium containing 10% fetal calf serum at a volume ratio of 1:5 and incubate at 37 °C for 120 h. During this period, the particle size and PDI of E-PLNs were measured by a nanoparticle size analyzer every 24 h.

### **Cell culture**

The human MCF-7 and MCF-7/ADR cells were purchased from Jiangsu Kaiji Biotechnology Co., Ltd, Jiangsu, China. The cells were cultured in RPMI-1640 medium (Gibco, USA) containing 10% fetal bovine serum (Gibco, USA), 1% penicillin and streptomycin (Gibco, USA) at 37 °C in an incubator containing 5% CO<sub>2</sub>. 200 ng/mL DOX (Dalian Meilun Biotechnology Co., Ltd., Dalian, China) was added into the medium of MCF-7/ADR cells.

### **Resistance index and cell viability**

MCF-7 and MCF-7/ADR cells were inoculated into 96-well plates ( $4 \times 10^4$  cells/well) (Wuxi NEST Biotechnology Co. Ltd., Jiangsu, China) and treated with DOX with different concentrations for 48 h. The cell viability was determined by MTT assay. The optical density (OD) at 490 nm of the viable cells was obtained by Microplate Reader (BioTek, Synergy H1, VT, USA). The cell viability was calculated according to formula (3), and the resistance index (RI) of MCF-7/DOX cells was calculated according to formula (4). MCF-7/ADR cells were then treated with different concentrations of EMO or E-PLN combined with DOX for 48 h, and the cell viability was detected according to formula (3).

$$\text{Cell viability (\%)} = (\text{OD}_{\text{exp}} - \text{OD}_{\text{blank}}) / (\text{OD}_{\text{control}} - \text{OD}_{\text{blank}}) \times 100\% \quad (3)$$

$$\text{RI} = \text{IC}_{50\text{MCF-7/ADR}} / \text{IC}_{50\text{MCF-7}} \quad (4)$$

### **Apoptosis**

According to the protocol recommended by the reagent manufacturer, after treating MCF-7/ADR cells with drug-containing medium for 48 h, collect all cells, resuspend them in 500  $\mu\text{L}$  cell staining buffer, add 5  $\mu\text{L}$  Annexin V-FITC and 5  $\mu\text{L}$  PI solution (Beyotime Biotechnology Co., Ltd., Shanghai, China) to stain cells. Fluorescence was detected using a flow cytometer (BD, FACSCanto, NJ, USA).

### **Cell invasion**

200  $\mu\text{L}$  ( $5 \times 10^4$  cells/mL) of cells were added to the Matrigel-precoated upper chamber of the Transwell plate (Corning Incorporated, NY, USA) and cultured in drug-containing but serum-free medium. 500  $\mu\text{L}$  of drug-containing complete medium was added to the lower chamber. After 24 h of culture, the non-migrated cells on the upper side of the upper chamber were removed, and the migrated cells on the lower

side of the upper chamber were fixed with 4% paraformaldehyde, stained with crystal violet, and photographed under a microscope. The crystal violet was washed with 33% acetic acid solution, and the OD value of the eluate at 570 nm was detected using a microplate reader (BioTek, Synergy H1, VT, USA).

#### **Enzyme-linked immunosorbent (ELISA)**

Cells were seeded in 6-well plates at a density of  $3 \times 10^5$  cells/well. After 48 h of treatment with medicated medium, the supernatant was collected and filtered. According to the protocol recommended by the reagent manufacturer (Bioswamp, Wuhan, China), add the sample, biotin-labeled antibody, enzyme labeling reagent, cleaning agent, chromogenic reagent, and stop solution to the pre-coated 96-well plate at different times, using a microplate reader (BioTek, Synergy H1, VT, USA) to detect the OD value at 450 nm.

#### **Western blot assay**

Cells were seeded in 6-well plates and collected after treatment with drug-containing medium. RIPA lysis buffer containing enzyme inhibitors and phenylmethylsulfonyl fluoride was added to the cells to extract total protein, and the total protein concentration was measured using a BCA protein assay kit (Beyotime Biotechnology Co., Ltd., Shanghai, China). Mix the remaining sample and loading buffer at a ratio of 4:1 (V/V), heat at 100 °C for 3–5 min, aliquot and store in a -80 °C refrigerator. 5 µL (30 µg) of total protein was loaded into each well, separated by 12% Sodium dodecyl sulphate–polyacrylamide gel electrophoresis (SDS-PAGE) gel in an electrophoresis tank, and then transferred to a polyvinylidene difluoride (PVDF) membrane. The PVDF membrane was incubated overnight at 4 °C with primary antibody solution, washed with PBS solution containing Tween-20 (PBST), and then incubated with horseradish peroxidase (HRP)-conjugated secondary antibody for 2 h. Likewise, wash with PBST solution. Finally, ECL chemiluminescent chromogenic solution (Beijing 4A Biotech Co. Ltd., Beijing, China) was added to the PVDF membrane and detected by a chemiluminescence imaging system. Grayscale values were analyzed using Image J software. Antibodies of GAPDH, Vimentin, E-cadherin, N-cadherin, Bax, Bcl-2, Fas, P53, P-gp, MRP1, JAK2, p-JAK2, STAT3 and p-STAT3 and HRP-conjugated secondary antibody were purchased from Abcam Plc, Cambridge, U.K.

#### **Statistical analysis**

The numerical data were presented as the mean  $\pm$  standard deviation (SD). Data analysis was performed using IBM SPSS software. Unpaired two-tailed t test and one-way analysis of variance (ANOVA) followed by the Bonferroni post hoc test were used for statistical significance analysis. The images were drawn by GraphPad Prism 6.0, Origin and Adobe Photoshop software. All experiments were repeated three times. \* $p < 0.05$ , \*\* $p < 0.01$ , \*\*\* $p < 0.001$ .  $p < 0.05$  was considered statistically significant, and ns means no significance.

## Results

### The physicochemical properties of E-PLNs

The appearance of the prepared E-PLNs dispersion is shown in Fig. 1A. The dispersion was a clear yellow liquid with opalescent light. The appearance of the freeze-dried E-PLNs powder is shown in Fig. 1B. The powder was yellowish granular or lumpy with fluidity. The peak areas of different concentrations of EMO standard solutions were determined by HPLC. The linear regression analysis was carried out based on EMO concentrations and corresponding peak areas, and the linear regression equation of EMO was obtained as  $y = 35.917x + 8.3615$  ( $R^2 = 0.9999$ ). EMO solution had good linearity in the concentration range of 0.781 ~ 50.0  $\mu\text{g/mL}$ . Three batches of E-PLNs samples were prepared, and the EE and LE were calculated according to formula (1) and (2). The results are shown in Table 1. The EE of the prepared E-PLNs was high, but the LE was low. The particle size of E-PLNs was  $(123.1 \pm 0.32)$  nm, the Zeta potential was  $(-28.6 \pm 0.23)$  mV, and the PDI was 0.135 ( $< 0.2$ ) (Fig. 1C, D). The particle size of E-PLNs in PBS, RPMI1640 and RPMI1640 solution containing 10% FBS showed no significant difference within 120 h (Additional file 1: Fig. S1), indicating good stability. The reason may be that a monolayer composed of PEGylated lipid molecules stabilizes the polymer core, thereby preventing nanoparticle aggregation.

The absorption peaks of EMO at 225, 290 and 450 nm were detected by ultraviolet spectrophotometer. Empty carrier PLNs had no absorption peak at the above three wavelengths. E-PLNs and the physical mixture of EMO and PLNs had absorption peaks at the above three wavelengths (Fig. 2A). The presence of EMO in E-PLNs was proved.

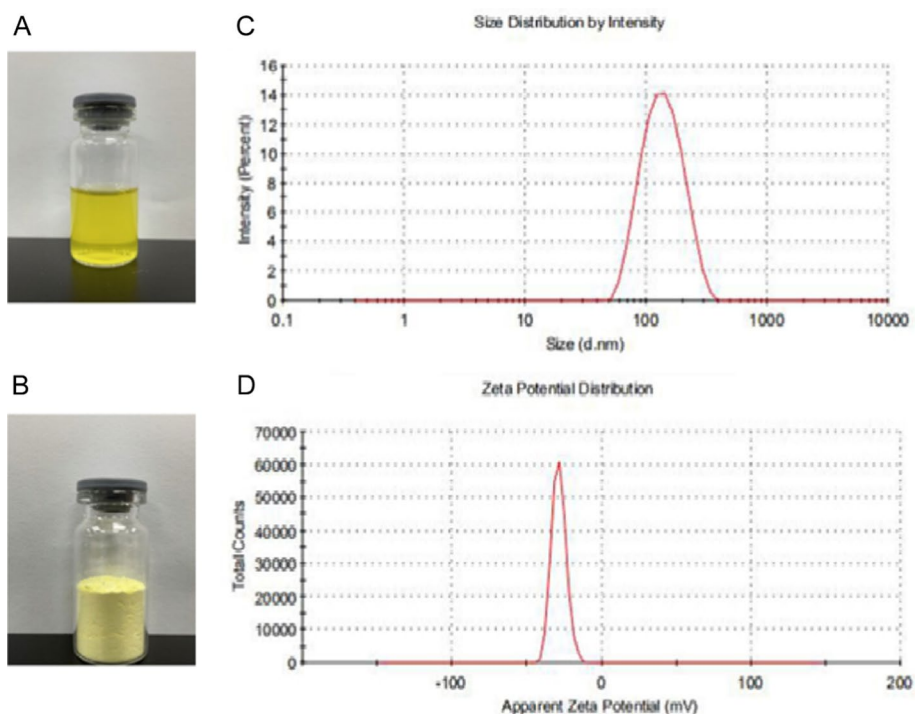


**Fig. 1** Representative pictures of the appearance, particle size and zeta potential of E-PLNs. **A** Appearance of a dispersion of E-PLNs; **B** Appearance of freeze-dried powder of E-PLNs; **C** Particle size distribution of E-PLNs; **D** Zeta potential distribution of E-PLNs

**Table 1** Encapsulation efficiency and loading efficiency of E-PLNs

Index	Experiment No	Value (%)	Average value (%)	Standard deviation (%)
EE (%)	1	75.72	74.75	1.68
	2	72.81		
	3	75.71		
LE (%)	1	2.13	2.15	0.02
	2	2.17		
	3	2.14		

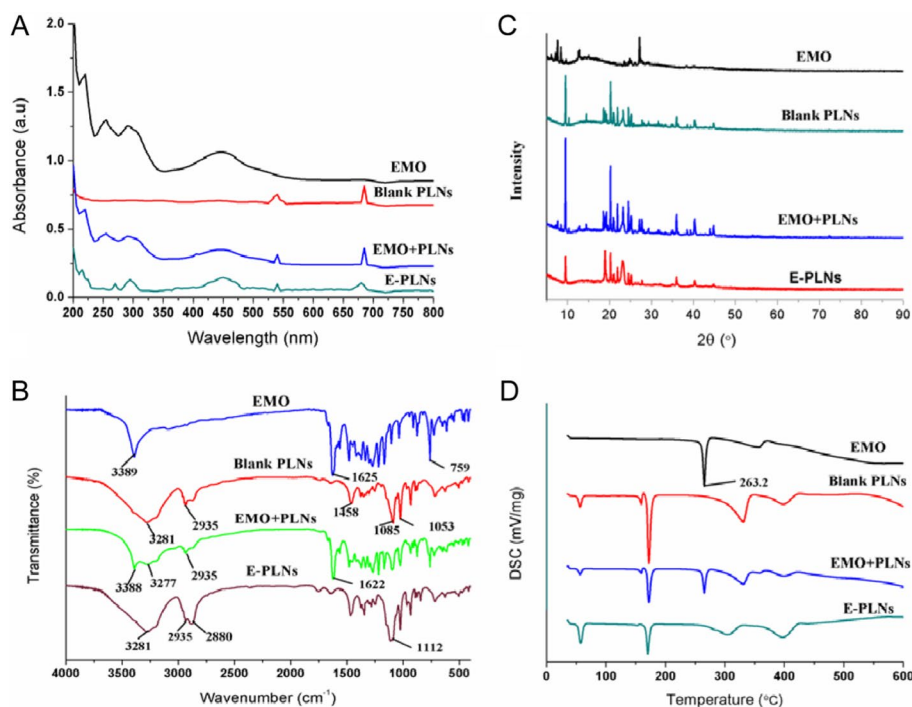


**Fig. 2** Characterization of the physicochemical properties of E-PLNs. **A** Ultraviolet absorption spectroscopy; **B** Fourier transform infrared absorption spectroscopy; **C** X-ray polycrystalline diffraction patterns; **D** Differential scanning calorimetry analysis.

In the EMO structure, the  $-OH$  group connected with the aromatic pentacorus had a characteristic peak at  $3389\text{ cm}^{-1}$ , the  $C=O$  functional group had a characteristic peak at  $1695\text{ cm}^{-1}$  and  $1596\text{ cm}^{-1}$ , and the aromatic  $C-H$  group had a characteristic peak at  $759\text{ cm}^{-1}$ . In PLNs, the  $-OH$  extension band of PLGA had a characteristic peak at  $3281\text{ cm}^{-1}$ , the  $C=O$  group of esters had a characteristic peak at  $1458\text{ cm}^{-1}$ , and the  $C-H$  and  $C-O$  extension band of DLPC had a characteristic peak at  $2935\text{ cm}^{-1}$  and  $1085\text{ cm}^{-1}$ . The spectra of the physical mixtures of EMO and PLNs could clearly distinguish PLNs from EMO, but the characteristic peaks of EMO were not found in the spectra of E-PLNs, indicating that EMO was encapsulated in E-PLNs (Fig. 2B).

The diffraction peaks of EMO at  $9.94^\circ$ ,  $13.27^\circ$ ,  $14.53^\circ$ ,  $22.49^\circ$ ,  $26.40^\circ$  and  $28.56^\circ$  were obtained by XRD, indicating that EMO existed in the form of crystallization. PLNs

also had several strong diffraction peaks, indicating that the excipients themselves existed in the form of crystallization. The diffraction peaks of EMO could be clearly distinguished in the EMO and PLNs physical mixture atlas, indicating that EMO and PLNs were simple physical mixtures. The diffraction peak of EMO in E-PLNs was not obvious, indicating that EMO was wrapped in E-PLNs in an amorphous state (Fig. 2C).

DSC analysis showed that EMO had a distinct characteristic peak at 263.2 °C, indicating that EMO existed in crystalline form. PLNs had distinct characteristic peaks but did not affect EMO. E-PLNs had no absorption peaks at 263.2 °C (Fig. 2D). The results showed that EMO in E-PLNs disperses in amorphous state, which is consistent with XRD analysis.

#### **EMT was associated with MCF-7/ADR cells proliferation, invasion and MDR**

EMT has been reported to be closely associated with tumor cell invasion and drug resistance. Activation of EMT in cancer is often regulated by TGF- $\beta$  pathway, which is manifested by abnormal expression of EMT-related proteins E-cadherin, N-cadherin and Vimentin. The mesenchymal phenotype of MCF-7/ADR cells was identified (Additional file 2: Fig. S2A, B). Compared with MCF-7 cells, N-cadherin and Vimentin were significantly upregulated in MCF-7/ADR cells ( $p < 0.01$ ). MCF-7 cells were less invasive in the culture process, while MCF-7/ADR cells showed significantly stronger invasion ability, and more cells penetrated the filtration membrane ( $p < 0.001$ ) (Additional file 2: Fig. S2C, D).

Galunisertib is a small molecule inhibitor of TGF- $\beta$  receptor I (TGF- $\beta$ R1) kinase. It works by inhibiting the phosphorylation of Smad and can selectively inhibit TGF- $\beta$  signal transduction and EMT in vitro. (Song et al. 2019). We verified the relationship between EMT and drug resistance through pharmacological inhibition based on Galunisertib. MCF-7/ADR cells were treated with Galunisertib (Beyotime Biotechnology Co., Ltd., Shanghai, China), which was found to have toxic effects, with an IC<sub>50</sub> value of 248.2  $\mu$ M (Additional file 2: Fig. S2E). When the Galunisertib concentration was 30  $\mu$ M, the cell viability was greater than 90%, which means this concentration inhibits EMT but has not significant effect on the cell viability. So MCF-7/ADR cells were pre-treated with 30  $\mu$ M of Galunisertib and then treated with DOX at different concentrations (1.56–200  $\mu$ M). In this condition, the IC<sub>50</sub> value of DOX on MCF-7/ADR cells was 57.05  $\mu$ M (Additional file 2: Fig. S2F). In contrast, The IC<sub>50</sub> values of DOX on MCF-7 and MCF-7/ADR cells were 5.35  $\mu$ M, 124.1  $\mu$ M, respectively (Additional file 2: Fig. S2K). It was indicated that Galunisertib improved the sensibility of MCF-7/ADR cells to DOX. Comparing with the control group, 30  $\mu$ M of Galunisertib significantly upregulated E-cadherin and downregulated N-cadherin and Vimentin (Additional file 2: Fig. S2G, H) and decreased the invasion ability (Additional file 2: Fig. S2I, J) in MCF-7/ADR cells, which confirmed that it can effectively inhibit EMT in MCF-7/ADR cells. These results probably mean EMT is involved in the response of MCF-7/ADR cells to DOX treatment.

To further prove this speculation, we compared the effects of Galunisertib and DOX, alone and in combination, on proliferation, invasion and MDR in MCF-7/ADR cells. All the trials we currently conducted lay the groundwork for later elucidating the intervention role of nanoparticles. Therefore, here we still chose a concentration (10

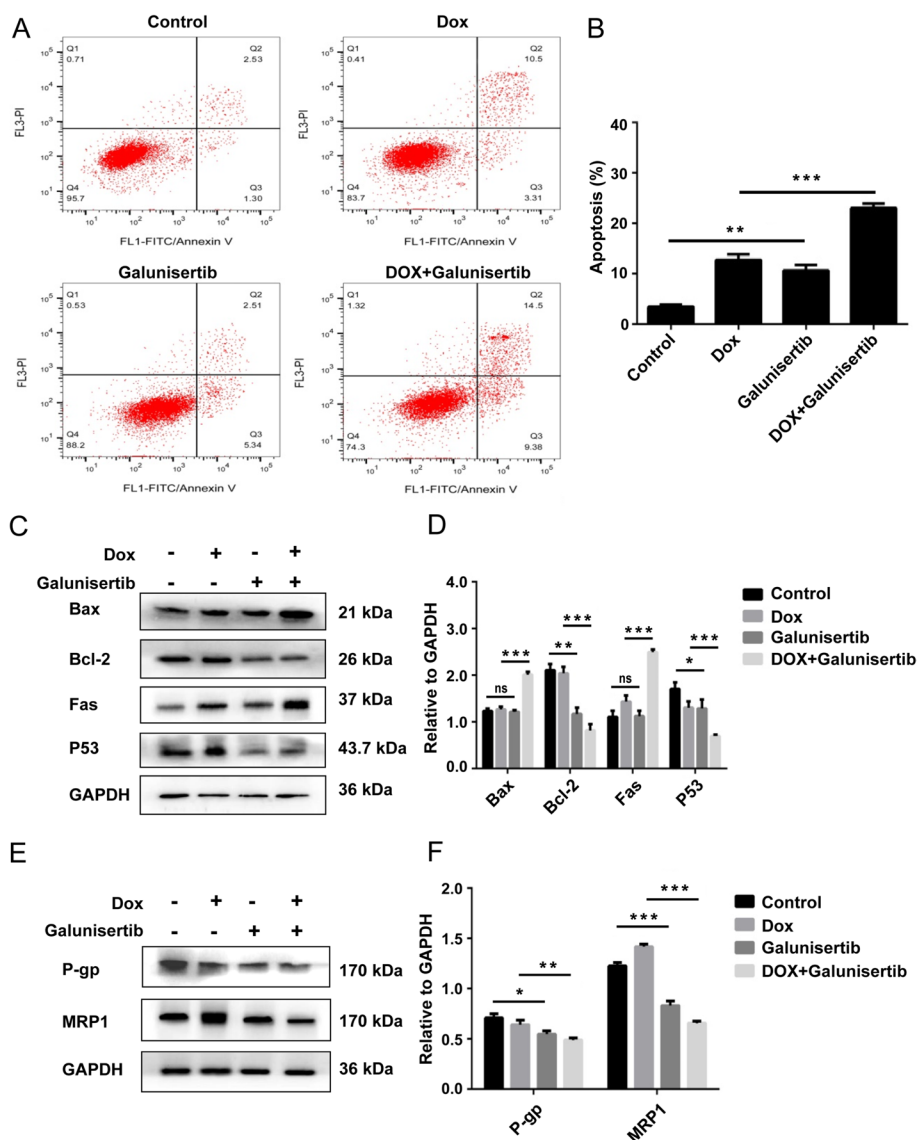


**Fig. 3** Relationship between EMT and apoptosis, MDR of MCF-7/ADR cell. **A** Detection of cell numbers at different times of apoptosis; **B** Apoptosis rates of each group; Annexin V-/PI- represents normal cells (a), Annexin V-/PI+ represents naked nuclei or mechanically damaged cells (b), Annexin V+/PI- represents early apoptotic cells (c), and Annexin V+/PI+ represents late apoptotic cells or necrotic cells (d). The cell apoptosis rate was defined as:  $(c + d) / (a + b + c + d) * 100\%$ . **C** Representative western blot bands of apoptosis related proteins; **D** The relative expression amounts of apoptosis related proteins; **E** Representative western blot bands of MDR related proteins; **F** Relative expression amounts of MDR related proteins. The numerical data (**B, D, F**) were presented as the mean  $\pm$  SD (n = 3). One-way ANOVA followed by the Bonferroni post hoc test (**B, D, F**) were used for statistical significance analysis. All experiments were repeated three times. \* $p < 0.05$ , \*\* $p < 0.01$ , \*\*\* $p < 0.001$ , ns means no significance.

$\mu\text{M}$ ) of DOX friendly to the viability of MCF-7/MDR cells. Compared with the control group, the apoptosis rate was increased (Fig. 3A, B), Bax and Fas proteins were upregulated (Fig. 3C, D), Bcl-2 and p53 proteins were downregulated (Fig. 3C, D), and P-gp and MRP1 proteins were downregulated (Fig. 3E, F) in MCF-7/ADR cells treated with 30  $\mu\text{M}$  Galunisertib; the apoptosis rate was increased (Fig. 3A, B), Fas proteins were

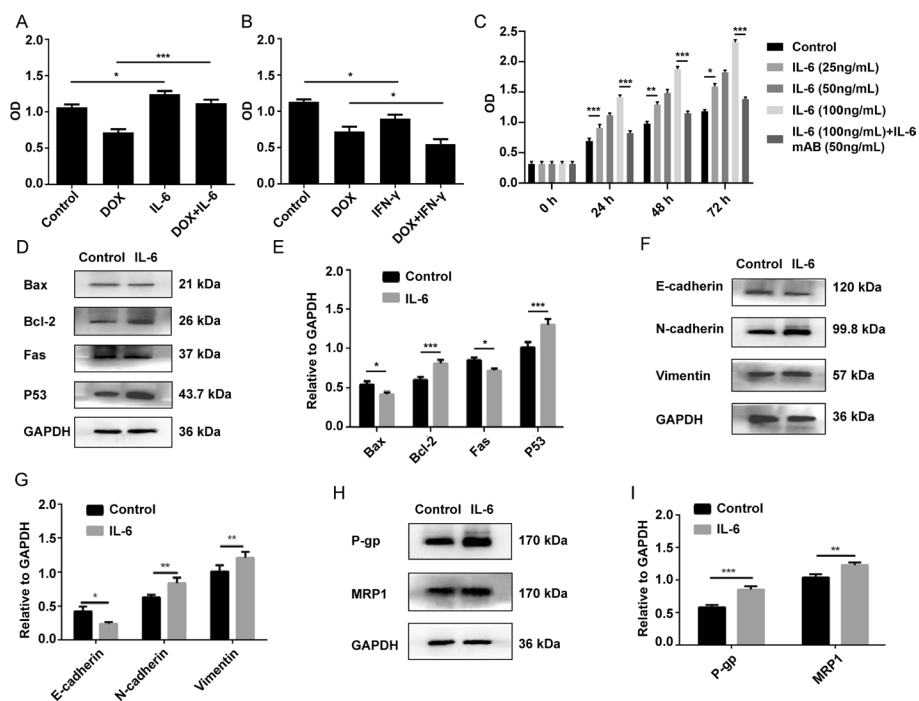


**Fig. 4** Relationship between IL-6 and proliferation, EMT and MDR of MCF-7/ADR cells. **A, C** Effects of IL-6 and its combination with DOX on the viability of MCF-7/ADR cells; **B** Effects of IFN-γ and its combination with DOX on the viability of MCF-7/ADR cells; **D, E** Effects of IL-6 on the expression of apoptosis related proteins in MCF-7/ADR cells; **F, G** Effects of IL-6 on the expression of EMT related proteins in MCF-7/ADR cells; **H, I** Effects of IL-6 on the expression of MDR related proteins in MCF-7/ADR cells. The numerical data (**A-D, F, H, J**) were presented as the mean ± SD (n = 3). Unpaired two-tailed t test (**A, F, H, J**) and one-way ANOVA followed by the Bonferroni post hoc test (**B-D**) were used for statistical significance analysis. All experiments were repeated three times. \**p* < 0.05, \*\**p* < 0.01, \*\*\**p* < 0.001.

upregulated (Fig. 3C, D), p53 proteins were downregulated (Fig. 3C, D), and MRP1 protein was upregulated (Fig. 3E, F) in MCF-7/ADR cells treated with 10 μM DOX. Compared with DOX or Galunisertib group, the combination of 10 μM DOX with 30 μM Galunisertib decreased the invasive ability of MCF-7/ADR cells (Figure S2I, J), improved the apoptotic rate (Fig. 3A, B), upregulated Bax and Fas protein, downregulated Bcl-2 and p53 protein (Fig. 3C, D), and downregulated P-gp with MRP1 protein (Fig. 3E, F). The results showed that Galunisertib could enhance the sensitivity of MCF-7/ADR cells to DOX by inhibiting EMT.

#### IL-6/JAK2/STAT3 signaling pathway mediates proliferation, EMT, and MDR in MCF-7/ADR cells

Overexpression of IL-6 in the microenvironment and its important role in growth, metastasis and therapeutic resistance has been demonstrated in various tumors, including BC (Masjedi et al. 2018). In addition to IL-6, cytokines such as IFN-γ are also closely related to drug resistance of tumor cells and can also activate downstream STAT signals (Legrier et al. 2016). However, in vitro culture supernatant assays revealed Expression level of IFN-γ in MCF-7/ADR cells compared with MCF-7 cells was not significantly higher, whereas IL-6 secretion was significantly higher (Additional file 2: Fig. S2L). To

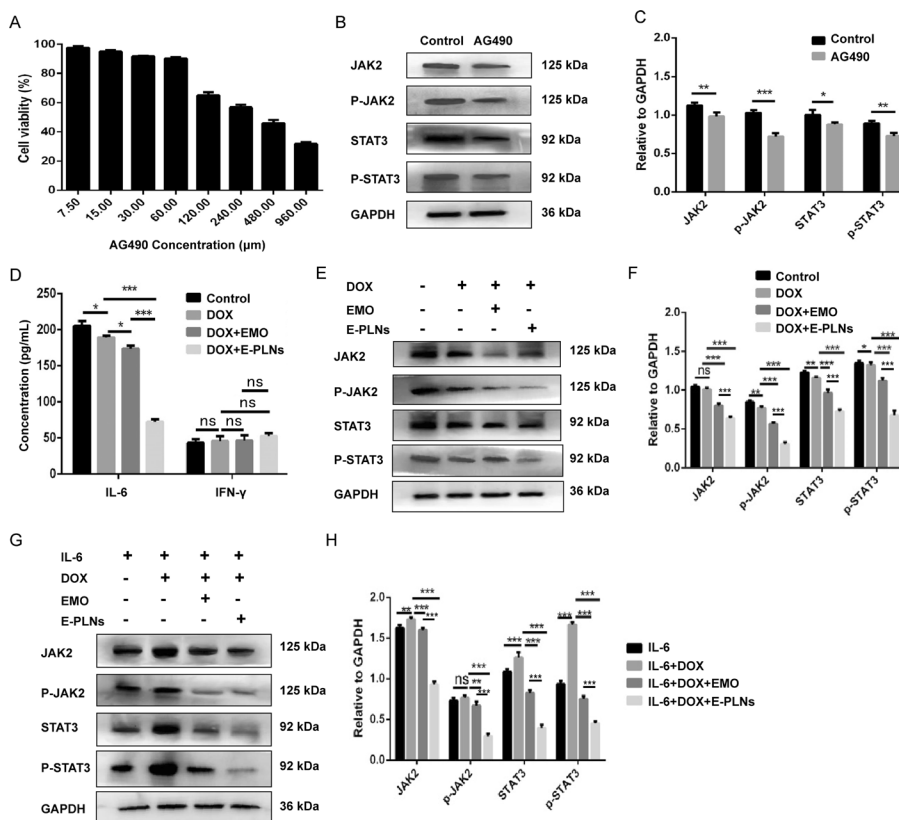


**Fig. 5** Effects of AG490 and E-PLNs on IL-6/JAK2/STAT3 signaling pathway in MCF-7/ADR cells. **A**, Effects of different concentrations of AG490 on viability of MCF-7/ADR cells; **B**, **C**, Effects of 40  $\mu$ M AG490 treatment on the expression of IL-6/JAK2/STAT3 signaling pathway in MCF-7/ADR cells; **D**, Effects of E-PLNs on the level of secretion of IL-6 and IFN- $\gamma$  in MCF-7/ADR cells; **E–H**, Effects of E-PLNs on the expression of IL-6/JAK2/STAT3 signaling pathway in MCF-7/ADR cells. The numerical data (A, C, D, F, H) were presented as the mean  $\pm$  SD ( $n = 3$ ). Unpaired two-tailed t test (**C**) and one-way ANOVA followed by the Bonferroni post hoc test (**D**, **F**, **H**) were used for statistical significance analysis. All experiments were repeated three times. \* $p < 0.05$ , \*\* $p < 0.01$ , \*\*\* $p < 0.001$ , ns means no significance.

determine the effects of IL-6 and IFN- $\gamma$  on the proliferation of BC drug resistant cells, MCF-7/ADR cells were treated with 25 ng/mL IL-6 and IFN- $\gamma$ , respectively. Compared with the control group, exogenous IL-6 treatment was beneficial to the proliferation of MCF-7/ADR cells, while exogenous IFN- $\gamma$  treatment was unfavorable to the proliferation of MCF-7/ADR cells (Fig. 4A, B). Compared with DOX group, IL-6 combine DOX group improved cell vitality, and IFN- $\gamma$  combine DOX group decreased the cell vitality (Fig. 4A, B). Although the study was designed to demonstrate the promoting effect of IL-6 on the proliferation of MCF-7/ADR cells, we unexpectedly found the inhibitory effect of IFN- $\gamma$  on the proliferation of MCF-7/ADR cells.

Next, MCF-7/ADR cells were treated with different concentrations (25, 50, 100 ng/mL) of IL-6 for 0, 24, 48, 72 h (Fig. 4C). The results showed that the vitality of MCF-7/ADR cells increased in a concentration-dependent manner during the incubation time range, and the proliferation rate was the fastest when cultured for 24 h. Besides, when IL-6 neutralizing antibody was added, cell proliferation was significantly reduced. Compared with the control group, inducing of 100 ng/mL of IL-6 for 24 h increased the expression

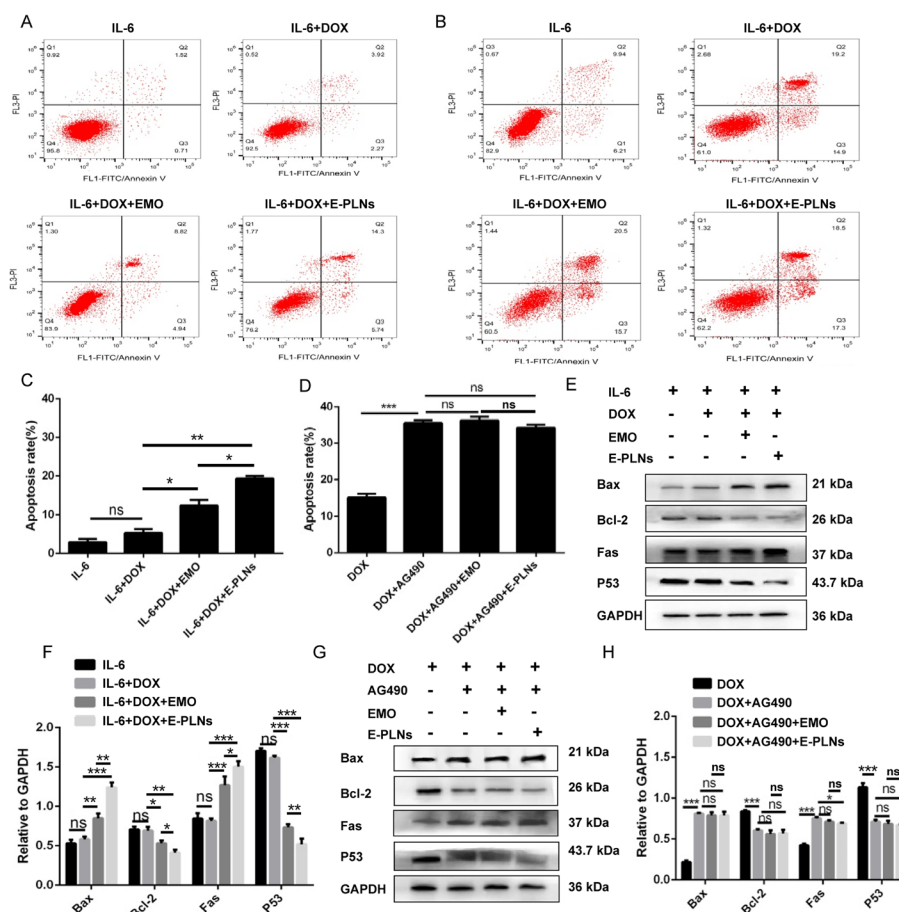


**Fig. 6** E-PLNs reversed IL-6 induced apoptosis resistance of MCF-7/ADR cells. A-D. Cells were pretreated with IL-6 or AG490, and the percentage of apoptotic cells was determined by flow cytometry; Annexin V-/PI- represents normal cells (a), Annexin V-/PI+ represents naked nuclei or mechanically damaged cells (b), Annexin V+/PI- represents early apoptotic cells (c), and Annexin V+/PI+ represents late apoptotic cells or necrotic cells (d). The cell apoptosis rate was defined as:  $(c + d)/(a + b + c + d) \times 100\%$ . E-F. Cells were pretreated with IL-6 or AG490, and the expression of apoptosis related proteins was determined by western blot. The numerical data (C, D, F, H) were presented as the mean  $\pm$  SD ( $n = 3$ ). One-way ANOVA followed by the Bonferroni post hoc test (C, D, F, H) were used for statistical significance analysis. All experiments were repeated three times. \* $p < 0.05$ , \*\* $p < 0.01$ , \*\*\* $p < 0.001$ , ns means no significance.

of antiapoptotic-related proteins Bcl-2 and P53, EMT-related proteins N-cadherin and Vimentin, and MDR-related proteins P-gp and MRP1 in MCF-7/ADR cells (Fig. 4D-I).

AG490 is a tyrosine kinase inhibitor that inhibits activity of JAK2/STAT3 signaling pathway, which is known as the downstream response original for IL-6 (Liu et al. 2022b). MCF-7/ADR cells were treated with different concentrations of AG490 (7.5–960  $\mu\text{m}$ ) for 48 h, and the cell viability decreased with the increase of concentration (Fig. 5A). When AG490 concentration was 50  $\mu\text{m}$ , the cell viability was greater than 90%, which could reduce the effect of AG490 on drug efficacy studies. Therefore, this concentration was chosen for the subsequent experiments. Compared with the control group, 50  $\mu\text{m}$  of AG490 downregulated the expression of JAK2/STAT3 pathway-related proteins in MCF-7/ADR cells, especially the expression of p-JAK2 and p-STAT3 proteins (Fig. 5B, C). Compared with the DOX group, AG490 combines DOX group increased

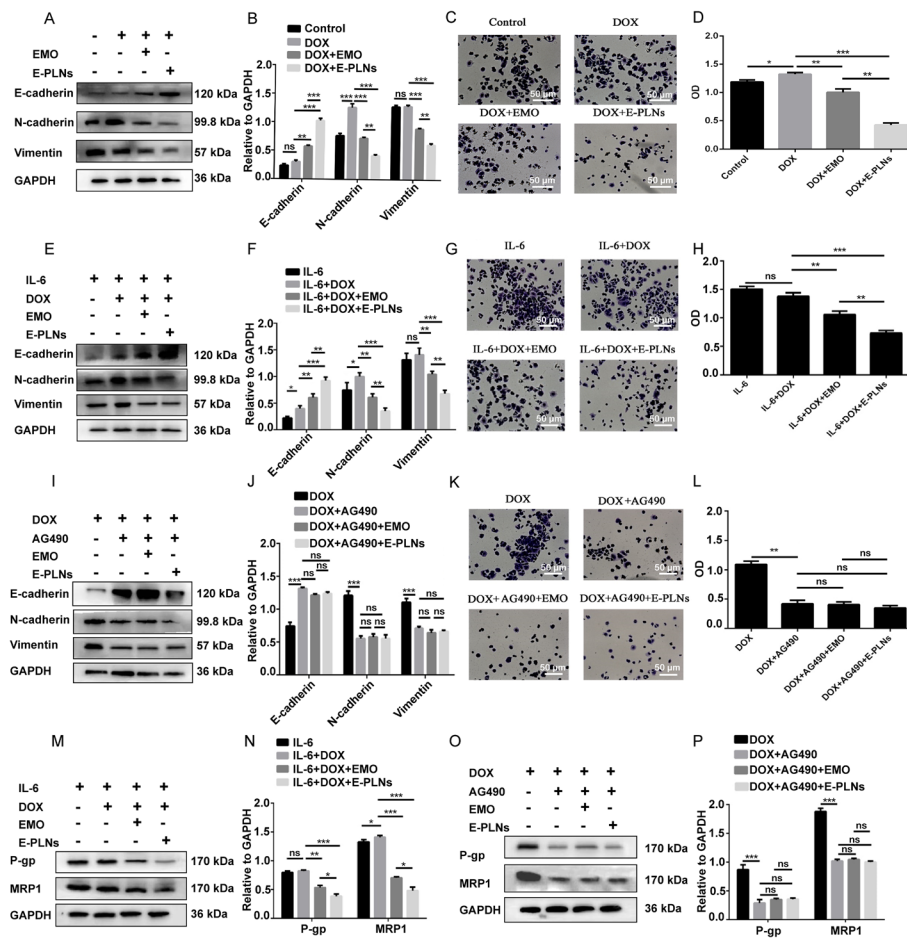


**Fig. 7** E-PLNs reversed IL-6 induced EMT, invasion and MDR of MCF-7/ADR cells. **A–B.** Expression of EMT related proteins under no pretreatment; **C–D.** Cell invasion under no pretreatment; **E–F.** Expression of EMT related proteins in the presence of IL-6; **G–H.** Cell invasion in the presence of IL-6; **I–J.** Expression of EMT-related proteins in the presence of AG490; **K–L.** Cell invasion in the presence of AG490. The numerical data (B, D, F, H, J, L, N, P) were presented as the mean  $\pm$  SD ( $n = 3$ ). One-way ANOVA followed by the Bonferroni post hoc test (B, D, F, H, J, L, N, P) were used for statistical significance analysis. All experiments were repeated three times. \* $p < 0.05$ , \*\* $p < 0.01$ , \*\*\* $p < 0.001$ , ns means no significance.

the apoptosis rate of MCF-7/ADR cells (Fig. 6B, D), upregulated the expression of Bax and Fas, downregulated the expression of Bcl-2 and p53 (Fig. 6G, H), decreased the invasive ability (Fig. 7K, L), upregulated the expression of E-cadherin protein, downregulated the expression of N-cadherin, Vimentin (Fig. 7I, J), and P-gp, MRP1 (Fig. 7O, P). The results confirmed that IL-6/JAK2/STAT3 signaling pathway plays an important role in MCF-7/ADR cell proliferation, EMT and MDR.

#### E-PLNs inhibited IL-6/JAK2/STAT3 signaling pathway activity in MCF-7/ADR cells

IL-6 activates JAK2/STAT3 signaling to promote proliferation, EMT and MDR in MCF-7/ADR cells, so how do E-PLNs affect this circuit? Firstly, we evaluated the effects of E-PLNs on the autocrine secretion levels of IL-6 and IFN- $\gamma$ . Compared with the DOX group, the secretion level of IL-6 was significantly inhibited in the DOX combine

E-PLNs group, while that of IFN- $\gamma$  did not change significantly (Fig. 5D). Next, we studied the effect of E-PLNs on the expression level of JAK2/STAT3 signaling pathway in MCF-7/ADR cells. The results showed that, compared with the control group, DOX had no significant effect on JAK2/STAT3 signaling pathway under normal conditions, while downregulated the expression of STAT3 and p-STAT3 when pre-incubated with 100 ng/mL of exogenous IL-6 for 24 h in MCF-7/ADR cells. Regardless of the addition of exogenous IL-6, the DOX + EMO and DOX + E-PLNs groups significantly downregulated the proteins expression levels of JAK2, p-JAK2, STAT3 and p-STAT3 in MCF-7/ADR cells compared with the DOX group, and the effect of DOX + E-PLNs was more significant (Fig. 5E–H). It was indicated that E-PLNs inhibited autocrine and paracrine IL-6 mediated IL-6/JAK2/STAT3 positive feedback loop in MCF-7/ADR cells.

#### **E-PLNs reversed IL-6 induced apoptosis resistance of MCF-7/ADR cells**

The MCF-7/ADR cells were pre-incubated with 100 ng/mL of IL-6 for 24 h, and then the groups were treated with DOX combine EMO or E-PLNs. Compared with the control group, DOX group had no significant influence on the apoptosis of MCF-7/ADR cells. Compared with the DOX group, apoptosis rate was significantly increased in the DOX + EMO and DOX + E-PLNs groups (Fig. 6A, C, E, F), and the expression of Bax and Fas was upregulated, while the expression of Bcl-2 and p53 were downregulated (Fig. 6E, F). Moreover, the pro apoptotic effect of E-PLNs was stronger than that of EMO. Using the JAK2/STAT3 inhibitor AG490 for validation, we found that, compared with the DOX group, DOX + AG490 group could promote the apoptosis of MCF-7/ADR cells; however, compared with the DOX + AG490 group, the apoptosis of DOX + AG490 + EMO or E-PLNs groups was not significantly increased, and only the expression of Fas protein was downregulated in DOX + AG490 + E-PLNs group (Fig. 6B, D, G, H). It was indicated that DOX induced apoptosis was inhibited by exogenous IL-6 in MCF-7/ADR cells, whereas the addition of AG490 or E-PLNs reversed or alleviated the IL-6-induced resistance to apoptosis.

#### **E-PLNs reversed IL-6 induced EMT and invasion of MCF-7/ADR cells**

The effects of E-PLNs on EMT and invasion of MCF-7/ADR cells were validated in three contexts. In the first context, cells were not pretreated and instead administered DOX, EMO, or E-PLNs directly. Compared with the control group, DOX group promoted the expression of N-cadherin and invasion, while DOX + EMO and DOX + E-PLNs groups downregulated the expression of N-cadherin and Vimentin, upregulated the expression of E-cadherin and inhibited invasion (Fig. 7A–D). In the second context, cells were pretreated with IL-6 and then administered DOX, EMO, or E-PLNs. Compared with the control group, DOX group promoted the expression of N-cadherin and E-cadherin. Compared with the control and DOX groups, DOX + EMO and DOX + E-PLNs groups downregulated the expression of N-cadherin and Vimentin, upregulated the expression of E-cadherin and inhibited invasion (Fig. 7E–H). In the third context, cells were pretreated with DOX and then administered AG490, EMO or E-PLNs. Compared with the control group, AG490, AG490 + EMO and AG490 + E-PLNs groups increased the expression of E-cadherin, decreased the expression of N-cadherin and Vimentin, and

inhibited invasion; however, these indexes showed no significant differences between the AG490 and AG490 + E-PLNs groups; effects of the AG490 + E-PLNs group was stronger than the AG490 + EMO group (Fig. 7I–L). The results suggested that E-PLNs combined with DOX could reverse IL-6 induced EMT and invasion in MCF-7/ADR cells, which had similar effects to AG490 but was probably based on independent mechanisms.

#### **E-PLNs reversed IL-6-induced MDR in MCF-7/ADR cells**

The effects of E-PLNs on the expression of drug resistant related proteins in MCF-7/ADR cells were detected in the presence of 100 ng/mL of IL-6 for 24 h. Compared with the control group, DOX group promoted the expression of MRP1, while DOX + EMO and DOX + E-PLNs groups suppressed the expression of P-gp and MRP1, and the suppression level was higher in DOX + E-PLNs group (Fig. 7M, N). The mechanism of E-PLNs was verified by pharmacological inhibition of JAK2/STAT3 signaling pathway using AG490. Compared with the DOX group, DOX + AG490 group significantly inhibited the expression of P-gp and MRP1 ( $p < 0.001$ ). However, compared with the DOX + AG490 group, the expression of P-gp and MRP1 had no obvious changes in DOX + AG490 + EMO or E-PLNs groups. The results showed that E-PLNs could inhibit IL-6-induced high expression of MRP1 or JAK2/STAT3 signaling pathway mediated high expression of MRP1 and P-gp, and thus reversed DOX resistance in MCF-7/ADR cells.

#### **Discussion**

In this study, polymeric lipid hybrid nanoparticles loaded with natural active ingredient EMO, namely E-PLNs, were prepared with small size and high drug encapsulation rate by emulsified solvent evaporation method. The physicochemical property assays demonstrated that EMO was encapsulated in the PLNs structure in an amorphous form (Liu et al. 2021c).

In our previous study (Liu et al. 2021c), RI and resistance-associated proteins assays were used to determine the insensitivity of MCF-7/ADR to treatment with DOX. We evaluated the effects of DOX combined with EMO or E-PLNs on the proliferation and MDR of MCF-7/ADR cells. The results showed that DOX combined with EMO or E-PLNs inhibited cell viability, induced apoptosis, promoted the expressions of pro-apoptotic genes Bax and Fas, inhibited the expressions of anti-apoptotic genes Bcl-2 and p53, increased cellular uptake of DOX, and inhibited the expression of P-gp and MRP1 in a dose-dependent manner. In addition, DOX combined with E-PLNs was superior to that with EMO, suggesting that the delivery of EMO using PLNs could improve its efficacy in inhibiting proliferation and drug resistance of MCF-7/ADR cells.

Many studies have confirmed the important role of EMT in the aggressiveness and drug resistance of BC (Hashemi et al. 2022). TGF- $\beta$  signaling is inhibited by binding to TGF- $\beta$ R II, phosphorylation of type I receptors, and subsequent phosphorylation activation of Smad2 and Smad3, with Phosphorylated SMad2/3 forming a trimer with Smad4, which then translocate to the nucleus and interacts with transcription factors, co-activators, and co-repressors to inhibit epithelial genes and promote the expression of mesenchymal protein (Park 2005). The EMT phenotypes of MCF-7 and MCF-7/ADR cells were analyzed, and it was confirmed that MCF-7/ADR cells had lower expression level

of E-cadherin, higher expression level of N-cadherin and Vimentin and stronger cell invasion ability. The use of Galunisertib (a TGF- $\beta$  signaling inhibitor) decreased MCF-7/ADR cell viability, upregulated the expression of E-cadherin, downregulated the expression of N-cadherin expression and Vimentin, and reduced cell invasion. In addition, Galunisertib also increased the apoptosis rate of MCF-7/ADR cells and downregulated the expression of anti-apoptotic proteins Bcl-2 and p53. The study confirmed that EMT was associated with the proliferation, EMT, invasion ability and MDR of MCF-7/ADR cells, which was consistent with the reported results.

The study of Ke et al. (Ke et al. 2011) found that the DNA fingerprint of the ADR-resistant MCF-7 cell subline (MCF-7/ADR') established by culturing parental MCF-7 cells with increasing concentrations of ADR was always consistent with the parental MCF-7 cells, whereas the DNA fingerprint of the established MCF-7/ADR cells (renamed NCI/ADR-RES) was not related to MCF-7 or MCF-7/ADR'. This indicates that MCF-7/ADR cells are not derived from MCF-7 breast cancer cells. Recent analysis suggests that NCI/ADR-RES cells are derived from OVCAR-8 ovarian adenocarcinoma cells, and the reasons behind this may be cell line cross-contamination and misidentification (Liscovitch and Ravid 2007). Therefore, when using MCF-7 and MCF-7/ADR paired cell models, it is necessary to identify the consistency of the origin before starting the study, or to use parental MCF-7 cells to re-introduce MCF-7/ADR cells. Or use other drug-resistant cell lines for comparison.

JAK and STAT are important components of many cytokine receptor systems, the most classic of which is the IL-6 (or gp130) receptor family. The IL-6/JAK2/STAT3 signaling pathway regulates many biological processes, including cell growth, survival, and differentiation. Abnormal feedback activation of IL-6 signaling and the downstream JAK2/STAT3 pathway has been found in a variety of cancers and is considered as a potential therapeutic target (Banerjee and Resat 2016). Excessive activation of STAT3 can promote the gene expression of CD44, cyclin D1, Bcl-2, Bcl-xL, Mcl-1, MMP, ERR $\alpha$ , VEGF, HIF-1 $\alpha$ , IL-10, TGF- $\beta$ , OCT-4, c-MYC, etc. These genes are related to stemness, cell cycle, apoptosis and survival, invasion and migration, angiogenesis, immunosuppression or chemoresistance of BC (Wong et al. 2022) (To et al. 2022). STAT3 can directly bind to the regulatory region within the TNFRSF1A gene, increase the transcription level of TNFRSF1A, and thereby regulate the NF- $\kappa$ B pathway (Egusquiaguirre et al. 2018). Targeting STAT3 signaling is a promising strategy for treating BC.

This study hypothesized that the proliferation, EMT, invasion and drug resistance of MCF-7/ADR cells were regulated by IL-6/JAK2/STAT3 signaling pathway. The results showed that MCF-7/ADR cells secreted higher levels of IL-6 than MCF-7 cells. Exogenous IL-6 increased MCF-7/ADR cell viability, decreased apoptosis rate, upregulated the expressions of anti-apoptotic proteins, downregulated the expressions of pro-apoptotic proteins, upregulated the expressions of EMT markers and MDR-related proteins and activated the JAK2/STAT3 signaling pathway. More importantly, the addition of exogenous IL-6 reduced the therapeutic effect of DOX on MCF-7/ADR cells. However, the use of JAK2/STAT3 signaling pathway inhibitor AG490 downregulated the expression of JAK2/STAT3 signaling pathway and reversed the above results induced by IL-6. The study confirmed that in addition to TGF- $\beta$  signaling, the IL-6/JAK2/STAT3 signaling pathway is also an important mechanism of EMT and invasion ability of MCF-7/ADR

cells, and regulates proliferation and MDR, which is a potential therapeutic target to overcome the MDR of MCF-7/ADR cells. In addition, an interesting finding during the study was that MCF-7/ADR cells secreted a lower level of IFN- $\gamma$  than MCF-7 cells, and exogenous IFN- $\gamma$  may play an inhibitory role in the proliferation of MCF-7/ADR cells.

In the present study, EMO or E-PLNs combined with DOX was found to reduce the secretion levels of IL-6 in MCF-7/ADR cells, while there was no significant effect on the secretion levels of IFN- $\gamma$ . Regarding whether the MCF-7/ADR cells were pre-incubated with IL-6 for 24 h before administration of each drug treatment group, EMO or E-PLNs combined with DOX significantly downregulated the expressions of JAK2, p-JAK2, STAT3, and p-STAT3 in MCF-7/ADR cells and the effect of E-PLNs was more obvious. The results suggested that EMO or E-PLNs can inhibit the production of IL-6 and induce the overexpression and activation of downstream JAK2/STAT3 signaling pathway, namely the IL-6-Jak2-STAT3 positive feedback loop, which is a potentially effective inhibitor of IL-6/JAK2/STAT3 signaling pathway. The downstream components of JAK2/STAT3 signaling pathway may also be involved in the EMT of BC cells and they may be the regulatory target of E-PLNs, which needs more experiments to prove.

MCF-7/ADR cells were pre-incubated with IL-6, and it was found that EMO or E-PLNs combined with DOX could reverse IL-6-induced enhancement of cell viability, apoptosis resistance, enhanced invasion ability, and elevated expression of EMT and MDR related proteins. The effect of E-PLNs was more obvious. The studies confirmed that EMO or E-PLNs can reverse the proliferation, EMT, invasion and DOX resistance in MCF-7/ADR cells by inhibiting the activity of IL-6/JAK2/STAT3 signaling pathway, thereby improving DOX efficacy. Delivery of EMO using PLNs may improve its efficacy at the molecular regulatory level. E-PLNs were a potentially effective chemotherapy sensitizer for BC. In addition, our study also found that the therapeutic effects of E-PLNs were similar to the TGF- $\beta$  signaling inhibitor Galunisertib, which means that E-PLNs may also be used as a potentially effective EMT inhibitor for the treatment of other diseases.

However, the assays in this study did not reach an all-round level. The expression levels of some marker proteins were not sufficient to reflect the degree of some acquired abnormal biological characteristics of cells. Combining real-time fluorescence quantitative PCR techniques to analyze the expression of EMT regulatory genes such as *Snail*, *ZEB1* and *Slug* mRNA, cytokine expression regulatory genes such as IL-6, and JAK2/STAT3 signaling pathway expression regulatory genes will be more conducive to confirming our conclusions (Xie et al. 2022). In addition, the ideal way to verify the biological function of IL-6/JAK2/STAT3 signaling pathway and the regulatory effect of E-PLNs was gene knockout or overexpression. The experimental grouping was also not well considered. The design should include groups using EMO and E-PLNs alone to understand the efficacy and mechanism of E-PLNs themselves on drug-resistant cells. Setting up groupings of at least three doses of drugs was necessary for both efficacy and mechanism studies. Considering the type and heterogeneity of tumors, different tumor drug resistant cell lines should be selected to explore the mechanism of tumor multidrug resistance and evaluate the applicability of E-PLNs. This study demonstrated that EMT was regulated by IL-6/JAK2/

STAT3 pathway in the process of BC drug resistance, but how IL-6/JAK2/STAT3 pathway regulates EMT and its relationship with TGF- $\beta$  were not clear. It was found that IFN- $\gamma$  inhibited the proliferation of MCF-7/ADR cells, and its relationship with EMT and drug resistance remains to be further clarified. The specific mechanism of E-PLNs in regulating IL-6/JAK2/STAT3 signaling pathway also needs to be further explored.

## Conclusion

In this study, polymeric lipid hybrid nanoparticles E-PLNs encapsulated with natural active ingredient EMO were prepared with small and uniform particle size, and good physicochemical properties for improving the water solubility and bioavailability of EMO. MCF-7/ADR cells derived from parental MCF-7 cells were used to study the mechanism of E-PLNs reversing drug resistance. Exogenous IL-6 and JAK2/STAT3 pathway inhibitors were used to confirm the involvement of IL-6 signaling and downstream JAK2/STAT3 pathway in the regulation of proliferation, EMT, invasion and MDR in MCF-7/ADR cells. TGF- $\beta$  inhibitors were used to investigate the relationship between EMT and MDR in MCF-7/ADR cells. EMO or E-PLNs combine with DOX could inhibit IL-6-induced over activation of JAK2/STAT3 pathway, proliferation, EMT, invasion and MDR, thereby reversing DOX resistance in MCF-7/ADR cells.

## Supplementary Information

The online version contains supplementary material available at <https://doi.org/10.1186/s12645-023-00237-z>.

**Additional file 1: Fig. S1.** Particle size change of E-PLNs in different solutions. Experiment was repeated three times. All data were expressed as the mean  $\pm$  SD (n = 3).

**Additional file 2: Fig. S2.** Relationship between EMT and proliferation, EMT and invasion ability of MCF-7 / ADR cells. A. Representative Western blot bands of EMT related proteins in MCF-7 versus MCF-7/ADR cells; B. Comparison of the relative expression amounts of EMT related proteins in MCF-7 versus MCF-7 / ADR cells; C. Transwell chamber assay was performed to detect the invasion ability of MCF-7 versus MCF-7/ADR cells; D. Optical density detection of MCF-7 versus MCF-7/ADR cells on the lower side of the upper chamber of Transwell using crystal violet staining; E. Effect of varying concentrations of galunisertib on viability of MCF-7/ADR cells; F. Effect of different concentrations of DOX on the viability of MCF-7/ADR cells after pretreatment with 30  $\mu$ M galunisertib; G. Representative Western blot bands of EMT related protein expression in MCF-7/ADR cells after 30  $\mu$ M galunisertib treatment; H. Relative expression of EMT related proteins in MCF-7/ADR cells after 30  $\mu$ M galunisertib treatment; I. Transwell chamber assay 30  $\mu$ M Galunisertib, 10  $\mu$ M DOX or the combination of the two treatments on the invasive ability of MCF-7/ADR cells; J. Optical density detection of MCF-7 / ADR cells on the lower side of the upper chamber of Transwell after 30  $\mu$ M Galunisertib, 10  $\mu$ M DOX or the combination of the two treatments. K. Cytotoxicity of DOX on MCF-7 and MCF-7/ADR cells. The numerical data (B, D, E, F, H, J) were presented as the mean  $\pm$  SD (n = 3). Unpaired two-tailed t test (B, D) and one-way ANOVA followed by the Bonferroni post hoc test (H, J) were used for statistical significance analysis. All experiments were repeated three times. \*\*p < 0.01, \*\*\*p < 0.001, ns means no significance.

## Author contributions

Honghui Gu and Fansu Meng conceived, designed the experiment, carried out the experiment and wrote draft. Honghui Gu, Fansu Meng, Lina Yang, Qi Li, and Zhong Chen, analyzed data, summarized results and participated in investigations. Haidong Sun, Tiange Cai, Zhenjiang Yang and Yu Cai, revised the manuscript and provided ideation guidance. Yu Cai conducted overall guidance for experiments. All authors read and approved the final manuscript.

## Funding

This work was supported by the [National Natural Science Foundation of China] under Grant [numbers 82274255, 82020108033, 82211540013, 82111540275]; the Fifth National Traditional Chinese Medicine Excellent Talents Training Program under Grant [number 2017–24]; and the [Sanming Project of Medicine in Shenzhen] under Grant [number 202211003].

## Availability of data and materials

All data and materials can be found in the article or in the supplementary materials, and more detailed data are available from the corresponding authors upon reasonable request.

## Declarations

### Ethical approval and consent to participate

Not applicable.

### Competing interests

The authors declare that they have no known competing financial interests or personal relationships that could have appeared to influence the work reported in this paper.

Received: 11 August 2023 Accepted: 7 December 2023

Published online: 31 January 2024

## References

- Banerjee K, Resat H (2016) Constitutive activation of STAT3 in breast cancer cells: a review. *Int J Cancer* 138(11):2570–2578
- Cheng M, Liu P, Xu LX (2020) Iron promotes breast cancer cell migration via IL-6/JAK2/STAT3 signaling pathways in a paracrine or autocrine IL-6-rich inflammatory environment. *J Inorg Biochem* 210:111159
- Dong X, Fu J, Yin X, Cao S, Li X, Lin L et al (2016) Emodin: a review of its pharmacology, toxicity and pharmacokinetics. *Phytother Res* 30(8):1207–1218
- Fisusi FA, Akala EO (2019) Drug combinations in breast cancer therapy. *Pharm Nanotechnol.* 7(1):3–23
- Fu M, Tang W, Liu J-J, Gong X-Q, Kong L, Yao X-M et al (2020) Combination of targeted daunorubicin liposomes and targeted emodin liposomes for treatment of invasive breast cancer. *J Drug Target.* 28(3):245–58
- Gote V, Nookala AR, Bolla PK, Pal D (2021) Drug resistance in metastatic breast cancer: tumor targeted nanomedicine to the rescue. *Int J Mol Sci* 22(9):4673
- Gottesman MM, Fojo T, Bates SE (2002) Multidrug resistance in cancer: role of ATP-dependent transporters. *Nat Rev Cancer* 2(1):48–58
- Hashemi M, Arani HZ, Orouei S, Fallah S, Ghorbani A, Khaledabadi M et al (2022) EMT mechanism in breast cancer metastasis and drug resistance: Revisiting molecular interactions and biological functions. *Biomed Pharmacother* 155:1
- Ji X, Lu Y, Tian H, Meng X, Wei M, Cho WC (2019) Chemoresistance mechanisms of breast cancer and their countermeasures. *Biomed Pharmacother.* 114:108800
- Ke W, Yu P, Wang J, Wang R, Guo C, Zhou L et al (2011) MCF-7/ADR cells (re-designated NCI/ADR-RES) are not derived from MCF-7 breast cancer cells: a loss for breast cancer multidrug-resistant research. *Med Oncol* 28(Suppl 1):S135-41
- Lan M, Kong Z, Liu F, Zou T, Li L, Cai T et al (2022) Activating Caspase-8/Bid/ROS signaling to promote apoptosis of breast cancer cells by folate-modified albumin baicalin-loaded nanoparticles. *Nanotechnology.* 33:43
- Legrier M-E, Bièche I, Gaston J, Beurdeley A, Yvonne V, Déas O et al (2016) Activation of IFN/STAT1 signalling predicts response to chemotherapy in oestrogen receptor-negative breast cancer. *Br J Cancer* 114(2):177–187
- Li B, Zhao X, Zhang L, Cheng W (2020) Emodin interferes with AKT1-mediated dna damage and decreases resistance of breast cancer cells to doxorubicin. *Front Oncol* 10:588533
- Li L, Zou T, Liang M, Mezhuiev Y, Tsatsakis AM, Đorđević AB et al (2021) Screening of metabolites in the treatment of liver cancer xenografts HepG2/ADR by psoralen-loaded lipid nanoparticles. *Eur J Pharm Biopharm Off J.* 165:337–44
- Liscovitch M, Ravid D (2007) A case study in misidentification of cancer cell lines: MCF-7/AdrR cells (re-designated NCI/ADR-RES) are derived from OVCAR-8 human ovarian carcinoma cells. *Cancer Lett.* 245(1–2):350–2
- Liu F, Li L, Lan M, Zou T, Kong Z, Cai T et al (2021a) Key factor regulating inflammatory microenvironment, metastasis, and resistance in breast cancer: interleukin-1 signaling. *Mediators Inflamm* 2021:7785890
- Liu F, Li L, Lan M, Zou T, Kong Z, Cai T et al (2021) Psoralen-loaded polymeric lipid nanoparticles combined with paclitaxel for the treatment of triple-negative breast cancer. *Nanomedicine* 16(27):2411–30
- Liu H, Zhuang Y, Wang P, Zou T, Lan M, Li L et al (2021) Polymeric lipid hybrid nanoparticles as a delivery system enhance the antitumor effect of emodin in vitro and in vivo. *J Pharm Sci* 110(8):2986–96
- Liu W, Wang X, Wang L, Mei Y, Yun Y, Yao X et al (2022) Oridonin represses epithelial-mesenchymal transition and angiogenesis of thyroid cancer via downregulating JAK2/STAT3 signaling. *Int J Med Sci* 19(6):965–74
- Liu F, Lan M, Ren B, Li L, Zou T, Kong Z et al (2022) Baicalin-loaded folic acid-modified albumin nanoparticles (FA-BSANPs/BA) induce autophagy in MCF-7 cells via ROS-mediated p38 MAPK and Akt/mTOR pathway. *Cancer Nanotechnol* 13(1):2
- Lüönd F, Sugiyama N, Bill R, Bornes L, Hager C, Tang F et al (2021) Distinct contributions of partial and full EMT to breast cancer malignancy. *Dev Cell* 56(23):3203–3221
- Masjedi A, Hashemi V, Hojjat-Farsangi M, Ghalamfarsa G, Azizi G, Yousefi M et al (2018) The significant role of interleukin-6 and its signaling pathway in the immunopathogenesis and treatment of breast cancer. *Biomed Pharmacother France* 108:1415–1424
- Park SH (2005) Fine tuning and cross-talking of TGF-beta signal by inhibitory Smads. *J Biochem Mol Biol* 38(1):9–16
- Ponnusamy L, Kothandan G, Manoharan R (2020) Berberine and Emodin abrogates breast cancer growth and facilitates apoptosis through inactivation of SIK3-induced mTOR and Akt signaling pathway. *Biochim Biophys Acta Mol Basis Dis* 1866(11):165897
- Semwal RB, Semwal DK, Combrinck S, Viljoen A (2021) Emodin - a natural anthraquinone derivative with diverse pharmacological activities. *Phytochemistry* 190:112854
- Shen J, Wang M, Li F, Yan H, Zhou J (2022) Homeodomain-containing gene 10 contributed to breast cancer malignant behaviors by activating Interleukin-6/Janus kinase 2/Signal transducer and activator of transcription 3 pathway. *Bioengineered* 13(1):1335–1345
- Song B, Park S-H, Zhao JC, Fong K-W, Li S, Lee Y et al (2019) Targeting FOXA1-mediated repression of TGF-β signaling suppresses castration-resistant prostate cancer progression. *J Clin Invest* 129(2):569–82
- Waks AG, Winer EP (2019) Breast cancer treatment: a review. *Jama.* 321(3):288–300

- Wang L, Zhang F, Cui J-Y, Chen L, Chen Y-T, Liu B-W (2018) CAFs enhance paclitaxel resistance by inducing EMT through the IL-6/JAK2/STAT3 pathway. *Oncol Rep* 39(5):2081–2090
- Wang L, Zhan X, Shen X, Li M, Yang J, Yu W et al (2018) P16 promotes the growth and mobility potential of breast cancer both in vitro and in vivo: the key role of the activation of IL-6/JAK2/STAT3 signaling. *Mol Cell Biochem* 446(1–2):137–48
- Wong GL, Manore SG, Doheny DL, Lo H-W (2022) STAT family of transcription factors in breast cancer: pathogenesis and therapeutic opportunities and challenges. *Semin Cancer Biol* 86(Pt 3):84–106
- Wu Q, Yang Z, Nie Y, Shi Y, Fan D (2014) Multi-drug resistance in cancer chemotherapeutics: mechanisms and lab approaches. *Cancer Lett* 347(2):159–66
- Xie W, Jiang Q, Wu X, Wang L, Gao B, Sun Z et al (2022) IKBKE phosphorylates and stabilizes Snail to promote breast cancer invasion and metastasis. *Cell Death Differ* 29(8):1528–40
- Xu Y, Zhu Y, Yue Y, Pu S, Wu J, Lv Y et al (2020) Tamoxifen attenuates reactive astrocyte-induced brain metastasis and drug resistance through the IL-6/STAT3 signaling pathway. *Acta Biochim Biophys Sin* 52(12):1299–305
- Zou T, Lan M, Liu F, Li L, Cai T, Tian H et al (2021) Emodin-loaded polymer-lipid hybrid nanoparticles enhance the sensitivity of breast cancer to doxorubicin by inhibiting epithelial–mesenchymal transition. *Cancer Nanotechnol* 12(1):22

### Publisher's Note

Springer Nature remains neutral with regard to jurisdictional claims in published maps and institutional affiliations.

**Ready to submit your research? Choose BMC and benefit from:**

- fast, convenient online submission
- thorough peer review by experienced researchers in your field
- rapid publication on acceptance
- support for research data, including large and complex data types
- gold Open Access which fosters wider collaboration and increased citations
- maximum visibility for your research: over 100M website views per year

**At BMC, research is always in progress.**

Learn more [biomedcentral.com/submissions](https://biomedcentral.com/submissions)

